$C\,^1\Sigma^+$, $A\,^1\Sigma^+$, and $b\,^3\Pi_{0^+}$ states of LiRb

I. C. Stevenson,[1,*] D. B. Blasing,[2] Y. P. Chen,[1,2,3] and D. S. Elliott[1,2,3]

[1]*School of Electrical and Computer Engineering, Purdue University, West Lafayette, Indiana 47907, USA*

[2]*Department of Physics and Astronomy, Purdue University, West Lafayette, Indiana 47907, USA*

[3]*Purdue Quantum Center, Purdue University, West Lafayette, Indiana 47907, USA*

We present the first spectroscopic studies of the $C\,^1\Sigma^+$ electronic state and the $A\,^1\Sigma^+$–$b\,^3\Pi_{0^+}$ complex in ^{7}Li-^{85}Rb. Using resonantly enhanced, two-photon ionization, we observed $v = 7, 9, 12, 13$, and 26–45 of the $C\,^1\Sigma^+$ state. We augment the REMPI data with a form of depletion spectra in regions of dense spectral lines. The $A\,^1\Sigma^+$–$b\,^3\Pi_{0^+}$ complex was observed with depletion spectroscopy, depleting to vibrational levels $v = 0 \rightarrow 29$ of the $A\,^1\Sigma^+$ state and $v = 8 \rightarrow 18$ of the $b\,^3\Pi_{0^+}$ state. For all three series, we determine the term energy and vibrational constants. Finally, we outline several possible future projects based on the data presented here.

I. INTRODUCTION

Ultracold polar molecules have been of great interest for many years. They have many applications in quantum logic operations, many-body effects, and collision studies at extremely low energies [1–3]. Due to the permanent electric dipole moment of these molecules in their rovibrational ground state, the long-range anisotropic interaction between neighbors allows a range of unique physical interactions [4,5] that are inaccessible to ultracold atomic systems. The most recent addition to the bi-alkali-metal family of ultracold molecules is ^{7}Li-^{85}Rb [6–8]. Recent work on this system has revealed a high rate of photoassociation (PA) [6] and a pathway for direct generation of ground rovibronic molecules through PA and spontaneous decay [9]. Much of this work makes use of a resonantly coupled 2(1)-4(1) state for PA [9]. We have also observed short-range PA through the $d\,^3\Pi_\Omega$ states, leading to population in the low-lying vibrational levels of the metastable $a\,^3\Sigma^+$ state [10].

In order to achieve many of the goals for ultracold polar molecules, it is essential to generate and confine a large number of molecules. For generation, trapping, and control of the molecules, we must explore the various electronic potentials, with special interest in singlet-triplet mixed states that can be useful in transferring population from triplet to singlet states (or vice versa). In the present work, we explore the $C\,^1\Sigma^+$, $A\,^1\Sigma^+$, and $b\,^3\Pi_{0^+}$ states, all previously unexplored in LiRb. For each of these potentials we determine the term energies and vibrational constants. With the exploration of the levels discussed in the present work, only one low-lying electronic state has not yet been studied, the $c\,^3\Sigma^+$ state. In Table I we list the 11 lowest-energy states of the LiRb system and the vibrational levels that have been observed for each.

In the past, our spectroscopic studies of LiRb [7,9,12,14] have been driven by our goal of producing large numbers of ultracold molecules in the rovibronic ground state. Our work here is no different; we evaluate possible stimulated Raman adiabatic passage (STIRAP) schemes through the $C\,^1\Sigma^+$ spectra for the transfer of population from loosely bound singlet molecules, produced at a high rate via PA [9,15],

to low vibrational levels of the $X\,^1\Sigma^+$ state. For v between 20 and 25 of the $C\,^1\Sigma^+$ state, the calculated Franck-Condon factors (FCFs) for both legs of this Raman transition are favorable. This forms an ideal transfer pathway in LiRb. We also evaluate various vibrational levels of the $A\,^1\Sigma^+$ state, which have played a key role in our previous determination [9] of the vibrational distribution of population in the $X\,^1\Sigma^+$ ground state. As part of this study, we find and evaluate strong spin-orbit coupling for certain vibrational levels of the $A\,^1\Sigma^+$–$b\,^3\Pi_{0^+}$ complex. Finally, the present measurements of higher vibrational levels of the $b\,^3\Pi_{0^+}$ state narrow a future search for the lowest several vibrational levels. Two possible applications for these mixed states are a direct molecular laser cooling scheme [16,17] and short-range photoassociation to produce ground-state molecules. The relevant potential energy curves (PECs) for this work are shown in Fig. 1 from Ref. [18].

The structure of this paper is as follows. In Sec. II we provide the relevant details of our experimental setup. In Sec. III, we present and discuss our data on the $C\,^1\Sigma^+$ electronic state. In Sec. IV, we present our data on the $A\,^1\Sigma^+$ and $b\,^3\Pi_{0^+}$ states. In Sec. V, we present our findings on $A\,^1\Sigma^+$–$b\,^3\Pi_{0^+}$ mixing. Finally in Sec. VI, we conclude and provide an outlook for future experiments on LiRb.

II. EXPERIMENTS

We work out of a dual-species magneto-optical trap (MOT), trapping $\sim 5 \times 10^7$ Li atoms and $\sim 2 \times 10^8$ Rb atoms in a cloud $\lesssim 1$ mK in temperature and 1 mm in diameter [7]. Our Rb MOT is a spatial dark spot MOT [19]. We photoassociate Li and Rb atoms to form LiRb molecules using a 150-mW external-cavity diode laser, which we tune to the 4(1), $v = -16$, $J = 1$ mixed state at $\nu_a = 12\,574.85$ cm^{-1} [9]. Spontaneous decay from the PA state forms bound LiRb molecules in many vibrational levels of the $X\,^1\Sigma^+$ ground state. We use v and J (without a prime) to denote the vibrational and rotational levels of the PA resonances (and for these vibrational numbers, we count down from the asymptote using negative integers), v' and J' to denote vibrational and rotational labeling of other excited electronic states, and v'' and J'' to denote the vibrational and rotational levels of the $X\,^1\Sigma^+$ state.

We use resonantly enhanced multiphoton ionization to ionize these molecules, which we detect with a time-of-flight

----

*istevens@purdue.edu

TABLE I. List of low-lying states of LiRb that have been observed experimentally. Ranges of vibrational quantum numbers followed with an asterisk are not inclusive. Weakly bound vibrational levels of many of these potentials used for photoassociation of ultracold LiRb molecules are not included.

Electronic state	Vibrational levels observed	Ref. No.(s.)	Atomic asymptote
$X\,^1\Sigma^+$	0–45	[11,12]	Li $2s\,^2S$+
$a\,^3\Sigma^+$	2–13*	[7,10,11]	Rb $5s\,^2S$
$b\,^3\Pi$	9–19	This work	
$A\,^1\Sigma^+$	0–29	This work	Li $2s\,^2S$+
$c\,^3\Sigma^+$	–	–	Rb $5p\,^2P$
$B\,^1\Pi$	0–22	[8,12,13]	
$C\,^1\Sigma^+$	7–13*, 26–44	This work	
$D\,^1\Pi$	0–15	[8,13,14]	Li $2p\,^2P$+
$d\,^3\Pi$	0–22	[14]	Rb $5s\,^2S$
$f\,^3\Pi$	0–10	[7]	Li $2s\,^2S$+
$g\,^3\Sigma^+$	0–5	[7]	Rb $4d\,^2D$

spectrometer and microchannel plate detector. The laser used to drive the ionization process is a Nd:YAG pumped, pulsed dye laser. This laser is tunable in the wavelength range between 550 and 583 nm when loaded with an R590 dye ($\nu_c = 18\,150$–$17\,150$ cm^{-1}) or between 662 and 709 nm ($\nu_c = 15\,100$–$14\,100$ cm^{-1}) when loaded with an LDS 698
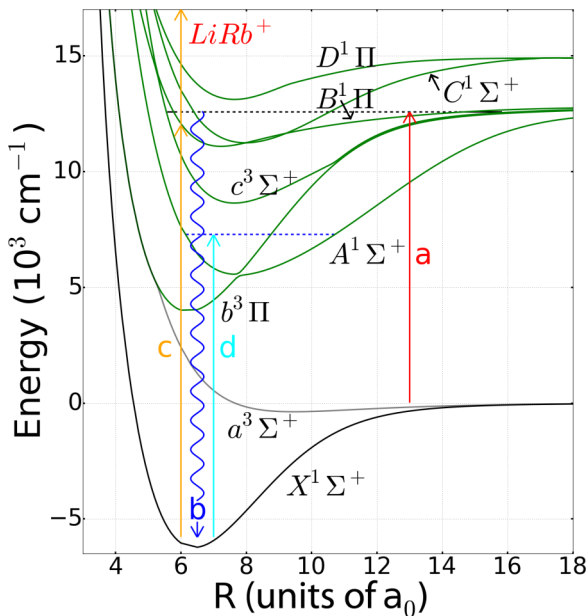

FIG. 1. Energy level diagram for the LiRb molecule showing relevant PECs from Ref. [18]. Vertical lines show various optical transitions, including (a) photoassociation of molecules below the Rb D_1 asymptote; (b) spontaneous decay of excited-state molecules leading to a wide range of $X\,^1\Sigma^+$ vibrational levels, drawn for $v'' = 2$; (c) REMPI to ionize LiRb molecules, labeled ν_c in other figures; and (d) excitation to deplete the REMPI signal. The dashed black line represents the 2(1)-4(1) PA resonance, while the dashed blue line represents the depletion state.

dye. The repetition rate of this laser is 10 Hz, and it delivers $\sim$3 mJ/pulse to the MOT region in a 4-mm-diameter beam. When the frequency of this laser is one-photon resonant with a transition from a state that is populated by spontaneous decay from the PA state to an intermediate bound state (usually one of the vibrational levels of the $C\,^1\Sigma^+$, $B\,^1\Pi$, or $D\,^1\Pi$ electronic potentials), absorption of two photons ionizes the molecule. The second step in this ionization process can be driven by the dye laser pulse (that is, one-color ionization, which we designate REMPI) or by the 532-nm pump laser pulse (two-color ionization, which we call RE2PI). In the latter case, we decrease the dye laser pulse energy to $\sim$0.5 mJ and adjust the timing between the two pulses to optimize the ionization signal. The frequency resolution of REMPI or RE2PI features is $\sim$0.5 cm^{-1}, limited by the line width of the pulsed dye laser.

We also use a form of depletion spectroscopy to augment our RE2PI studies. In this technique, we add a CW narrow-band depletion laser to the configuration. As demonstrated in Refs. [9,20], the depletion laser reduces the REMPI ion count by resonantly transferring population from the active initial state in REMPI to other bound states. Our depletion laser is a 300-mW CW Ti:sapphire laser that we tune between 740 and 905 nm. We copropagate the PA and depletion lasers and then focus them to a spot size of about 200 μm in diameter in the center of the MOTs. Depletion spectroscopy has a high spectral resolution, limited primarily by the uncertainty of our wave meter, 0.02 cm^{-1}.

The population distribution of the initial states limits the excited states accessible with the depletion laser. Since the ground-state molecules are mostly in the $J'' = 0$ rotational state [9], selection rules allow optical transitions to $J' = 1$ rotational states. Transitions from $J'' = 2 \rightarrow J' = 1$ or 3 are barely detectable above the shot-noise level, so we are unable to determine the rotational constants of the excited state. Additionally, we are limited by the spin of our molecules starting in the $X\,^1\Sigma^+$ state. For transitions to $b\,^3\Pi_\Omega$, where $\Omega = 0^+, 0^-, 1$, and 2, only $\Omega = 0^+$ peaks appear in the spectra, borrowing strength from the nearby $A\,^1\Sigma^+$ vibrational levels. Ω is the projection of the total electronic angular momentum (orbital plus spin) onto the internuclear axis. Transitions to $\Omega = 0^-$ or 2 are not allowed. Transitions to $\Omega = 1$ are possible due to second-order spin-orbit mixing with mixed $A\,^1\Sigma^+$–$b\,^3\Pi_{0^+}$ states, but they are too weak to observe.

Besides shot noise in the ion count, two sources of uncertainty in depletion peak positions deserve mention: frequency drifts of both the PA laser and the REMPI laser. The PA laser frequency was maintained with an electronic lock. Drift in the REMPI laser frequency was small, slow, and nearly linear, so we were able to compensate in postprocessing. Therefore, the primary limitation to the precision of these measurements was the shot noise in the signal.

III. $C\,^1\Sigma^+$ DISCUSSION

We make use of the population in the $v'' = 42$ and 43 levels of the $X\,^1\Sigma^+$ state, formed by spontaneous decay after the PA step, to record the positions of the $v' = 26$–45 vibrational lines of the $C\,^1\Sigma^+$ state. To detect these molecules we use RE2PI with the LDS 698 dye in the dye laser, which ionizes the molecules through the loosely bound vibrational levels of
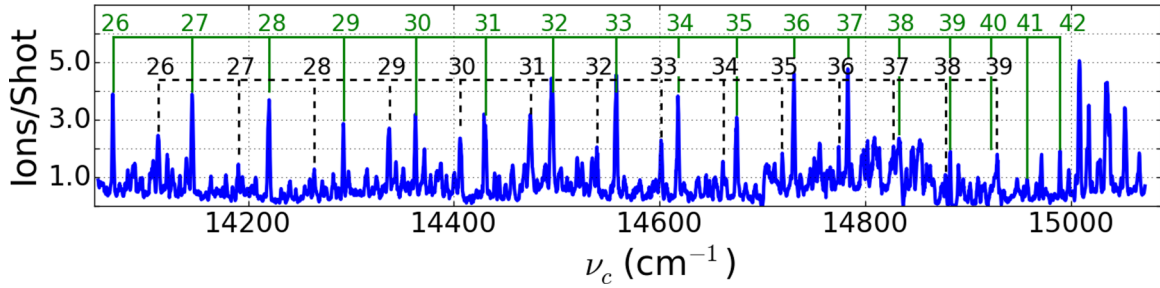
FIG. 2. RE2PI spectra from $v'' = 42$ and 43 to the $C\,^1\Sigma^+$ electronic state. Solid green lines and numbers label transitions $C\,^1\Sigma^+\ v' \leftarrow v'' = 43$; dashed black lines and numbers label transitions $C\,^1\Sigma^+\ v' \leftarrow v'' = 42$.

the $C\,^1\Sigma^+$ electronic state. Thus we are able to measure the energies of the vibrational levels of the $C\,^1\Sigma^+$ state relative to $v'' = 42$ and 43.

As part of our work here, we measured the binding energies of $v'' = 42$ and $v'' = 43$ with the highest precision to date. In this project we measured the frequency of the depletion transition $B\,^1\Pi$, $v' = 20 \leftarrow X\,^1\Sigma^+$, $v'' = 43$ to be 12 711.71 (0.02) cm^{-1} [4(1), $v = -16$ is the Hund's case (c) labeling of the $B\,^1\Pi$, $v' = 20$ state]. In Ref. [9], the binding energy of 4(1), $v = -16$, $J = 1$ was measured to be 12 574.85 (0.02) cm^{-1}; the difference between these two frequencies gives us the binding energy, $v_{43} = -136.86$ (0.02) cm^{-1}. This is in good agreement with, but of a higher precision than, the measurements in Refs. [11,12], which measured a binding energy of $v_{43} = -137$ (4) cm^{-1}. Additionally using our RE2PI spectra in Fig. 2, we extracted the energy difference between $v'' = 42$ and $v'' = 43$ to be 44.1 (0.1) cm^{-1}, which compares favorably to the more accurate energy difference from Refs. [11,12], 44.04 cm^{-1}.

We show the RE2PI spectrum of $v' = 26$–42 of the $C\,^1\Sigma^+$ state in Fig. 2. Two progressions dominate, one from $v'' = 42$ and the other from $v'' = 43$. They are spaced by 44.1 cm^{-1}, precisely the energy difference between $v'' = 42$ and $v'' = 43$ [12]. We show these series in Fig. 2 with dashed black lines and solid green lines, respectively. The integers indicate our assignments of the intermediate RE2PI state, which is a vibrational level v' of the $C\,^1\Sigma^+$ state. The weak, unlabeled RE2PI lines in this spectrum originate from $v'' = 38$–41, which are also populated by the PA resonance we used. These qualitative features are consistent with the calculation of the FCF for the spontaneous decay from the PA state to $X\,^1\Sigma^+$,

which yields values for $v'' = 43$ and 42 (0.35 and 0.13, respectively) much greater than those for any other vibrational level [9]. For frequencies significantly below the Rb $5S$ + Li $2P$ asymptote, the line density of the spectrum in Fig. 2 is very low, allowing us to measure the energies of $v' = 26$–40 twice, thus resulting in a $0.5/\sqrt{2} = 0.3$ cm^{-1} precision of the mean.

As the $v'' = 43$ series converges on the Rb $5S$ + Li $2P$ asymptote, line congestion increases. This occurs near $v_c = v_{D_1} + |v_{43}| \simeq 15\,050$ cm^{-1}, where $v_{D_1} = 14\,904$ cm^{-1} is the frequency of the atomic Li D_1 line. To assign these peaks we used depletion spectroscopy to identify sets of RE2PI peaks that share a common initial state, as shown in Fig. 3. For these data, the solid blue trace is the original data from Fig. 2, while the dashed red trace is the RE2PI data retaken in the presence of a depletion laser driving the $B\,^1\Pi\ v' = 20 \leftarrow v'' = 43$ transition. The peaks originating from $v'' = 43$ (shown by the solid green and dot-dashed green lines in Fig. 3) largely vanish upon the introduction of the depletion laser. Careful inspection of Fig. 3 shows that all the strong peaks disappear after we introduce the depletion laser; this is consistent with the picture told by FCFs; that is, there is three times more population in $v'' = 43$ than in $v'' = 42$. The peak for the $C\,^1\Sigma^+\ v' = 45 \leftarrow v'' = 43$ is tentative, since the energy of this peak is above the asymptote. Still, we note that the peak is strongly depleted by the depletion laser, the spacing is about right for this progression, and the long-range potential for the $C\,^1\Sigma^+$ PEC is expected to be repulsive [18], that is, $C_6 < 0$, which could lead to a quasibound state above the asymptote. The $D\,^1\Pi$ potential from Ref. [13] provides a good guide in this region, with an average uncertainty of 2.5 cm^{-1}, which allows us to identify candidate lines for transitions to the $C\,^1\Sigma^+$
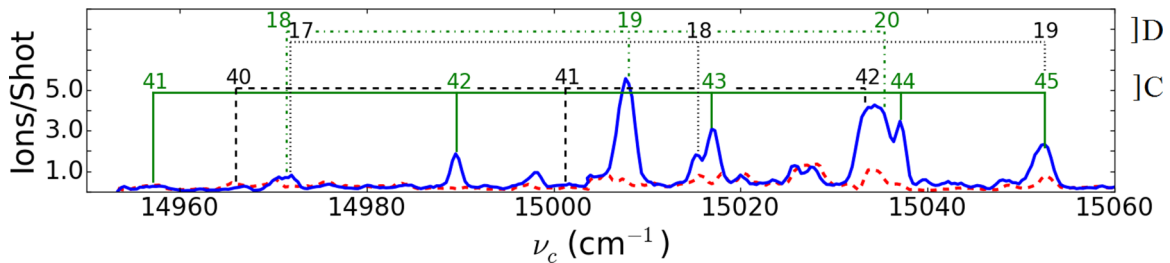

FIG. 3. Depletion spectroscopy of RE2PI data on transitions from $v'' = 42$ and 43 to the $C\,^1\Sigma^+$ and $D\,^1\Pi$ electronic states. For these data, the solid blue trace represents the original data from Fig. 2; the dashed red trace, the RE2PI data retaken in the presence of a depletion laser driving the $B\,^1\Pi\ v' = 20 \leftarrow v'' = 43$ transition. Reduction of a peak height in the presence of the depletion laser indicates that the initial state is $v'' = 43$. Assignments of these lines are labeled as follows: solid green lines, $C\,^1\Sigma^+ \leftarrow v'' = 43$; dashed black lines, $C\,^1\Sigma^+ \leftarrow v'' = 42$; dotted black lines, $D\,^1\Pi \leftarrow v'' = 42$; and dot-dashed green lines, $D\,^1\Pi \leftarrow v'' = 43$.

TABLE II. Measured vibrational energies of the $C\,^1\Sigma^+$ electronic state. The uncertainty in T_v is 0.5 cm^{-1} for $v' = 7$–13 and 40–45 and is 0.3 cm^{-1} for $v' = 26$–39. The vibrational numbering was chosen to smoothly connect to the deeply bound vibrational levels measured in Ref. [13]. Energies are referenced to the Rb 5S + Li 2S atomic asymptote.

v'	T_v (cm^{-1})	ΔE (cm^{-1})
7	12131.2	
9	12344.2	
12	12655.8	102.4
13	12758.2	
26	13931.3	77.6
27	14008.9	74.4
28	14083.2	72.5
29	14155.7	69.5
30	14225.3	68.3
31	14293.6	64.8
32	14358.4	62.3
33	14420.6	60.0
34	14480.6	57.3
35	14537.9	55.5
36	14593.4	52.6
37	14646.0	50.0
38	14696.0	49.9
39	14745.9	44.9
40	14784.9	38.9
41	14820.1	32.0
42	14852.1	27.8
43	14879.9	20.2
44	14900.1	15.4
45	14915.5	

state. The unassigned lines in Fig. 3 most likely result from $D\,^1\Pi$ $v' = 18$–$20 \leftarrow v'' = 38$–41 transitions; these initial states are weakly populated by the PA resonance, and the calculated FCFs for these lines are strong.

For $v' < 13$, we used the R590 dye in the pulsed dye laser and excited from the $v'' = 2$ or 3 level of the ground state. Otherwise, the measurements were similar to those described above. The density of lines in these spectra was great enough to require depletion spectroscopy to make line assignments with confidence. Table II is a summary of our observed energies of the $v' = 7, 9, 12, 13$, and 26–45 vibrational levels of the $C\,^1\Sigma^+$ state.

There have been no previous direct observations of the $C\,^1\Sigma^+$ v' states. In Ref. [13], the authors observed perturbations to the rotational lines of the $B\,^1\Pi \leftarrow X\,^1\Sigma^+$ spectrum, from which they extracted the binding energies of $C\,^1\Sigma^+$, $v' \simeq$ 0–13 and calculated a $C\,^1\Sigma^+$ PEC. We see good agreement with the PEC in Ref. [13] for $v' < 13$. We fitted the $C\,^1\Sigma^+$, $v' = 7$–40 line positions listed in Table II to

$$T(v) = T_e + \omega_e(v + 1/2)$$
$$- \omega_e x_e(v + 1/2)^2 + \omega_e y_e(v + 1/2)^3, \qquad (1)$$

extracted both the term energy T_e and the vibrational constants, and made a smooth connection across the gap from $v' = 13$–26, which led to the vibrational numbering we report. The energies of states $v' = 41$–45 do not fit Eq. (1) well and were omitted from the fit. We present the term energy and molecular constants in Table III.

IV. $A\,^1\Sigma^+$ AND $b\,^3\Pi_{0+}$ DISCUSSION

In this section, we discuss a set of measurements in which we use depletion spectra to identify excited states. This is in contrast to the previous section, where we used depletion spectra only to identify common initial states. In total we deplete two REMPI transitions exciting deeply bound $X\,^1\Sigma^+$ ground states to the $A\,^1\Sigma^+$, $v' = 0$–29 and the $b\,^3\Pi_{0+}$, $v' = 8$–18 levels. For $A\,^1\Sigma^+$, $v' = 19$–29 states, we used $v'' = 10$ as the initial state for depletion and tuned the REMPI laser to the $D\,^1\Pi$ $v' = 4 \leftarrow v'' = 10$ transition. For $A\,^1\Sigma^+$, $v' = 0$–18 and $b\,^3\Pi_{0+}$, $v' = 8$–18 states, we used $v'' = 2$ as the initial state and tuned the REMPI laser to the $B\,^1\Pi$ $v' = 14 \leftarrow v'' = 2$ transition. We were unable to search for $v' < 8$ of $b\,^3\Pi_{0+}$, which fall outside the tuning range of our Ti:sapphire laser. The $A\,^1\Sigma^+$ and $b\,^3\Pi_{0+}$ series are readily distinguishable since the $A\,^1\Sigma^+$ lines are extremely power broadened. (For example, the line width of the $A\,^1\Sigma^+$ $v' = 2 \leftarrow v'' = 2$ transition was well in excess of 30 GHz for a depletion laser power of ∼100 mW.) In fact, their width greatly facilitated their search, with guidance from the *ab initio* calculations in Ref. [18]. Such broad line widths of the peaks allowed us to increment the depletion laser frequency in 10-GHz steps when searching for resonances. Then we made low-intensity measurements of the line positions to remove any line shifts caused by saturation effects. We tabulate the

TABLE III. Molecular constants fitted to our data, compared to fits of other experiments [13] or to theoretical predictions from *ab initio* calculations in Refs. [16] and [18]. State energies are given by Eq. (1). For fitting $C\,^1\Sigma^+$ we omitted $v' = 41$–45 because the energies of these states fall outside the range over which Eq. (1) is valid. When fitting $b\,^3\Pi_{0+}$, the vibrational numbering is uncertain since we have not observed $v' < 8$. We chose vibrational numbering to force a well depth between the two *ab initio* predictions. Additionally, we omitted $v' = 10, 12, 14$, and 16 from the fit because these levels are strongly perturbed, as shown in Fig. 4(b). For these data, the value of y_e is not significant and not included in the table.

	$C\,^1\Sigma^+$			$A\,^1\Sigma^+$		$b\,^3\Pi_{0+}$		
	Expt.	Expt. [13]	Theor. [18]	Expt.	Theor. [18]	Expt.	Theor. [18]	Theor. [16]
ω_e (cm^{-1})	115.4 (0.9)	113.8 (0.2)	113.4	117.3 (0.6)	117.9	195.1 (1.0)	190.6	188.3
$10^3 x_e$	3.1 (0.4)		2.3	3.1 (0.4)	3.3	4.3 (0.2)	2.9	3.4
$10^6 y_e$	−78 (5)		−87	15 (9)	23		−18.4	−29.7
T_e (cm^{-1})	11 288 (13)	11 302 (4)	11 237.4	5756.6 (2.2)	5537.7	4083 (7)	3962.3	4180.4

TABLE IV. Experimental assignments for the location of $A\,^1\Sigma^+$, v', $J' = 1$ based on our depletion data. The uncertainty for all assignments is 0.02 cm^{-1}. Energies are referenced to the Rb $5S$ + Li $2S$ atomic asymptote.

v'	$T_v + 2B_v$ (cm^{-1})	ΔE (cm^{-1})
0	5808.10	122.52
1	5930.62	127.55
2	6058.17	104.47
3	6162.64	117.18
4	6279.82	106.67
5	6386.50	118.75
6	6505.25	111.78
7	6617.02	110.61
8	6727.63	111.01
9	6838.64	110.88
10	6949.52	106.71
11	7056.23	111.41
12	7167.64	110.58
13	7278.21	104.49
14	7382.65	110.04
15	7492.70	108.41
16	7601.10	104.31
17	7705.41	107.04
18	7812.45	105.84
19	7918.29	104.34
20	8022.63	104.44
21	8127.07	103.83
22	8230.90	103.14
23	8334.04	102.90
24	8436.95	102.84
25	8539.78	100.67
26	8640.45	101.80
27	8742.26	101.80
28	8844.06	97.97
29	8942.03	

TABLE V. Experimental assignments for the location of $b\,^3\Pi_{0^+}$, v', $J' = 1$ based on our depletion data. The uncertainty for assignments is 0.02 cm^{-1}; the vibrational designation is approximate. Energies are referenced to the Rb $5S$ + Li $2S$ atomic asymptote.

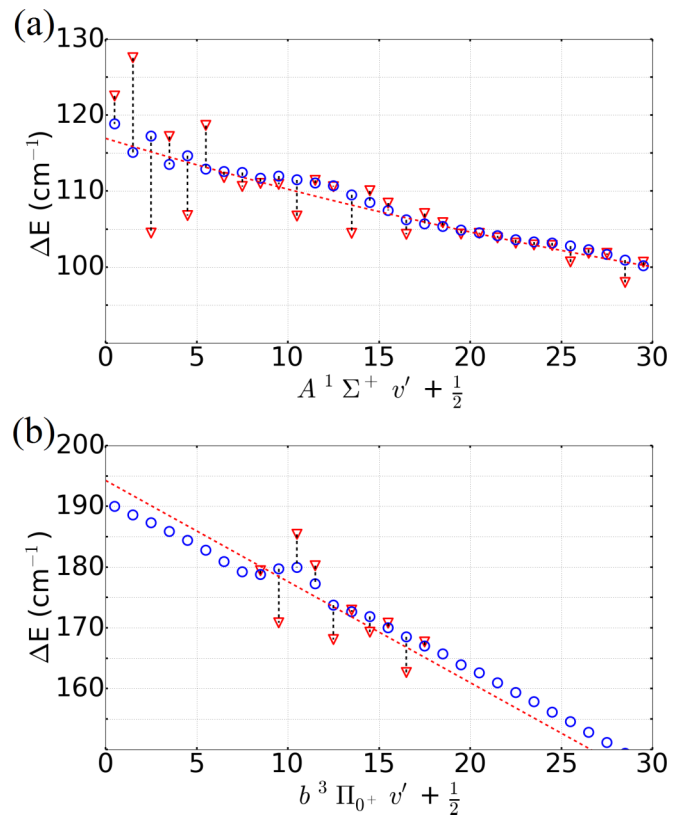| v'	$T_v + 2B_v$ (cm^{-1})	ΔE (cm^{-1})
8	5682.01	179.41
9	5861.42	170.83
10	6032.25	185.39
11	6217.65	180.22
12	6397.87	168.08
13	6565.95	172.92
14	6738.87	169.28
15	6908.16	170.78
16	7078.94	162.65
17	7241.59	167.68
18	7409.27	

FIG. 4. Comparison of theoretical vibrational spacings (blue circles) to our measurements (red triangles) for (a) $A\,^1\Sigma^+$ and (b) $b\,^3\Pi_{0^+}$. Dashed black vertical lines connect data sets to guide the eye. The dashed red line is the fit using Eq. (1) and the molecular constants listed in Table III. Large deviations in experiment vs theory are driven by perturbations. The unevenness of the theoretical predictions in the $v' = 0$–4 region for $A\,^1\Sigma^+$ and the $v' = 7$–12 region for $b\,^3\Pi_{0^+}$ is an artifact caused by imperfect conversion from adiabatic to diabatic PECs. Finally, we note that (b) suggests that our extracted constants, ω_e and x_e, for the $b\,^3\Pi_{0^+}$ state are too large. Our data for this state are limited, and it appears that if both were smaller, the fit would better match the theory (blue circles).

energies of the $A\,^1\Sigma^+$, v', $J' = 1$ states in Table IV, and the energies of the $b\,^3\Pi_{0^+}$, v', $J' = 1$ states in Table V.

In Fig. 4, we show the experimental and theoretical [18] energy spacing between the vibrational lines of the $A\,^1\Sigma^+$ series [Fig. 4(a)] and the $b\,^3\Pi_{0^+}$ series [Fig. 4(b)]. In this figure, red triangles represent the experimental data, blue circles show the theoretical data, vertical dashed black lines guide the eye between the two data sets, and dashed red lines are the plots of Eq. (1) with the molecular constants presented in Table III. In order to determine these points, we first converted the potential energy curves in Ref. [18] from adiabatic to diabatic [21] and then used LEVEL 8.0 [22] to calculate the positions of the $J' = 1$ eigenstate of the different vibrational levels. The vibrational line spacings of the $A\,^1\Sigma^+$ state that we observe show a smooth, gradual decrease for high vibrational states ($v' > 20$), as expected. For lower vibrational numbers, however, there are large shifts in several of the lines and moderate shifts in others. For example, the energy of the $v' = 2$ line is shifted up by $\sim$10 cm^{-1} above the general trend; in Fig. 4(a) this appears as $T_{v'=2} - T_{v'=1}$ is too large by nearly 10 cm^{-1}, while $T_{v'=3} - T_{v'=2}$ is too small by 10 cm^{-1}. Shifts of nearby vibrational lines, $v' = 10$ and 12, of the $b\,^3\Pi_{0^+}$ state

in the opposite direction suggest strong mixing between the $A\,^1\Sigma^+$ and the $b\,^3\Pi_{0^+}$ states through spin-orbit interactions. These perturbations recur over a rather large range of levels due to near-coincidence between three times the vibrational spacing of the $A\,^1\Sigma^+$ state and two times the vibrational spacing of the $b\,^3\Pi_{0^+}$ state. We discuss these perturbations in more detail in the next section. If we remove the most strongly perturbed vibrational states, the predicted vibrational spacings from the *ab initio* calculations are in good agreement with the remaining observed spacings. This is similar to our experience with other states in previous studies, such as the $d\,^3\Pi$ state [14], in which we found good general agreement between measured and calculated energy spacings between vibrational levels, but not with the well depth. This disagreement manifests itself through two fewer vibrational levels than predicted for the $A\,^1\Sigma^+$ v' series. In Table III, we present a direct comparison of the derived molecular constants from theory and our data, confirming our earlier assertion of excellent agreement.

V. $A\,^1\Sigma^+$–$b\,^3\Pi_{0^+}$ MIXING

In this section, we analyze state mixing between several vibrational levels of the $A\,^1\Sigma^+$ and the $b\,^3\Pi_{0^+}$ states. The two largest perturbations shown in Fig. 4(a) are due to mixing between the $A\,^1\Sigma^+$, $v'=2$ level and $b\,^3\Pi_{0^+}$, $v'=10$ and between the $A\,^1\Sigma^+$, $v'=5$ level and $b\,^3\Pi_{0^+}$, $v'=12$. The mixing between states is proportional to [23]

$$\frac{|\langle\Psi_{b\,^3\Pi}|H_{\mathrm{SO}}|\Psi_{A\,^1\Sigma^+}\rangle|^2}{\hbar\delta},\qquad(2)$$

where H_{SO} is the Hamiltonian for the spin-orbit interaction, and $\hbar\delta$ is the energy difference between the unperturbed states. The vibrational factor of the wave functions $|\Psi\rangle$ in this expression implies that strong state mixing requires large Franck-Condon overlap between two states, while the energy denominator requires a small energy difference. In Fig. 5, we show a rough estimate of the interaction strength caused by the spin-orbit effect divided by the state energy difference between the $A\,^1\Sigma^+$, $v'=2$, 5, 8 and 11 states and the various vibrational levels v' of the $b\,^3\Pi_{0^+}$ state. We estimate the interaction strength with [24] $V_{\mathrm{int}}=A_{\mathrm{Rb}}|\langle\Psi_{b\,^3\Pi}|\Psi_{A\,^1\Sigma^+}\rangle|^2/2$, where A_{Rb} is the spin-orbit interaction in atomic rubidium, $250\,\mathrm{cm}^{-1}$; we have found that this approximation roughly holds [14]. For $A\,^1\Sigma^+$, $v'=2$ and 5, mixing with one state is much stronger than any of the rest, justifying a two-state mixing model. The $A\,^1\Sigma^+$, $v'=8$ state is hardly perturbed because it has a very small Franck-Condon overlap with $b\,^3\Pi_{0^+}$, $v'=14$ despite having nearly identical energies. This is consistent with the story told by Fig. 4, as neither $A\,^1\Sigma^+$, $v'=8$ nor $b\,^3\Pi_{0^+}$, $v'=14$ appear significantly perturbed. Finally, Fig. 4(b) shows that $b\,^3\Pi_{0^+}$, $v'=16$ is slightly perturbed, by $A\,^1\Sigma^+$, $v'=10$ and 11, which matches the low interaction strength shown in Fig. 5(d).

For $A\,^1\Sigma^+$, $v'=2$ and 5, which we approximate as a simple two-state mixing model, we calculated the admixture coefficients. Using the treatment of mixed states in Ref. [23], we write the mixed states as

$$|\Psi_-\rangle = c|\Psi_{A\,^1\Sigma^+}\rangle - d|\Psi_{b\,^3\Pi}\rangle\qquad(3)$$
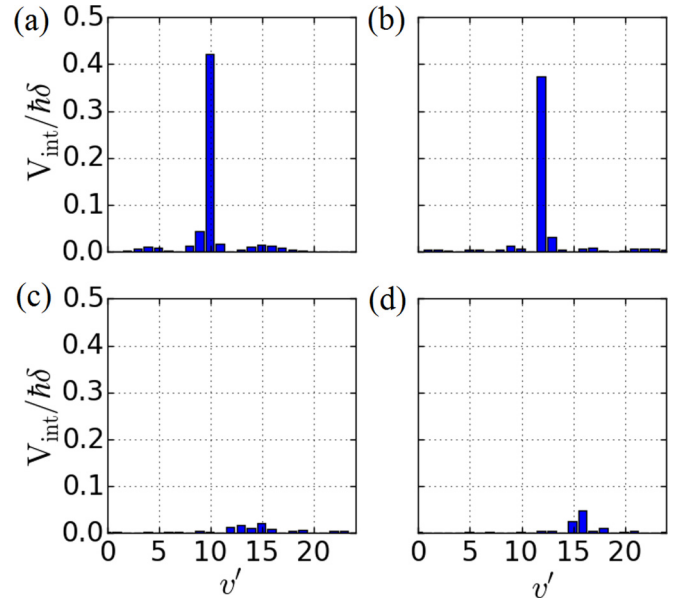

FIG. 5. Calculated $V_{\mathrm{int}}=A_{\mathrm{Rb}}|\langle\Psi_{b\,^3\Pi}|\Psi_{A\,^1\Sigma^+}\rangle|^2/2$, divided by the state energy difference, for $A\,^1\Sigma^+$ (a) $v'=2$, (b) $v'=5$, (c) $v'=8$, and (d) $v'=11$ interacting with the vibrational levels of the $b\,^3\Pi_{0^+}$ state. PECs are from Ref. [18], and we calculated the vibrational wave functions and FCFs using LEVEL8.0 [22]. $A_{\mathrm{Rb}}=250\,\mathrm{cm}^{-1}$ is the atomic rubidium spin-orbit constant.

and

$$|\Psi_+\rangle = d|\Psi_{A\,^1\Sigma^+}\rangle + c|\Psi_{b\,^3\Pi}\rangle,\qquad(4)$$

where $|\Psi_{A\,^1\Sigma^+}\rangle$ and $|\Psi_{b\,^3\Pi}\rangle$ are the bare states. The energies of states $|\Psi_-\rangle$ and $|\Psi_+\rangle$ are E_- and E_+, respectively. As we have done in the past [9], we can use the expected energy and observed energy of mixed states to estimate their mixing; we use the molecular constants in Table III to predict where the unperturbed state should lie. After we have a prediction for the unperturbed state location we can solve for the admixture coefficients

$$c^2 = \frac{1}{2}\left[1 - \frac{\hbar\delta}{E_+ - E_-}\right]\qquad(5)$$

and

$$d^2 = \frac{1}{2}\left[1 + \frac{\hbar\delta}{E_+ - E_-}\right].\qquad(6)$$

Additionally, we calculate the interaction strength, V_{int}, using $V_{\mathrm{int}}=\frac{1}{2}\sqrt{(E_+-E_-)^2-(\hbar\delta)^2}$ from Ref. [9]. All of the relevant parameters for the strongest mixed $A\,^1\Sigma^+$–$b\,^3\Pi_{0^+}$ states that we observe and the derived admixture coefficients and interaction strengths are listed in Table VI. For both of these states, V_{int} divided by FCF is within a factor of 2 of $A_{\mathrm{Rb}}/2$, showing approximate agreement with the model in Ref. [24]. These mixed states are critical for some future experiments, as discussed in the next section.

TABLE VI. Parameters of the mixed states. δ is the unshifted (bare) energy difference of the states, while $E_+ - E_-$ is the energy difference between the perturbed states. c and d are the admixture coefficients determined through Eqs. (5) and (6). V_{int} and/or FCF as determined through this analysis is in reasonable agreement with $A_{Rb}/2 = 125$ cm^{-1}, where A_{Rb} is the spin-orbit interaction strength in atomic rubidium.

$A\,{}^1\Sigma^+$ v'	$E - T_v$ (cm^{-1})	$b\,{}^3\Pi_{0^+}$ v'	$E - T_v$ (cm^{-1})	$\hbar\delta$ (cm^{-1})	$(E_+ - E_-)$ (cm^{-1})	$|c|$	$|d|$	V_{int} (cm^{-1})	FCF	$\frac{V_{int}}{FCF}$
2	10.5	10	−7.6	7.7	25.8	0.59	0.81	12.3	0.06	205
5	−4.5	12	6.1	0.7	11.3	0.68	0.73	5.6	0.03	187

VI. OUTLOOK

We performed spectroscopy on three electronic states in LiRb—$C\,{}^1\Sigma^+$, $A\,{}^1\Sigma^+$, and $b\,{}^3\Pi_{0^+}$—with the intention of using the data presented here to guide future work.

(1) In future work, we plan to explore $C\,{}^1\Sigma^+$, $v' = 22$ as an intermediate state for STIRAP to transfer population from $v'' = 43$ to $v'' = 0$. PA to the 2(1)-4(1) mixed state produces $v'' = 43$ molecules at a rate of $\approx 3 \times 10^5$ molecules per second. For future applications, we want to transfer these molecules to $v'' = 0$. As shown in Fig. 6, $C\,{}^1\Sigma^+$, $v' = 22$ is the best available state for this transfer if we use diode lasers based on calculated FCF's for the two legs of a STIRAP process, plus the availability of diode lasers. We observed vibrational levels $v' = 7$, 9, 12, 13, and 26–45 and saw very regular vibrational spacing. This is reflected in our harmonic constant, ω_e, which has an uncertainty of only 0.9 cm^{-1}. We were unable to reach $C\,{}^1\Sigma^+$, $v' = 22$ with the lasers we used for this experiment, but with the data presented here, depletion spectra should allow us to find $C\,{}^1\Sigma^+$, $v' = 22$ easily.

(2) We are interested in studying $b\,{}^3\Pi_{0^+}$, $v' = 0$–2; as suggested in Ref. [16], these states could be used to laser-cool
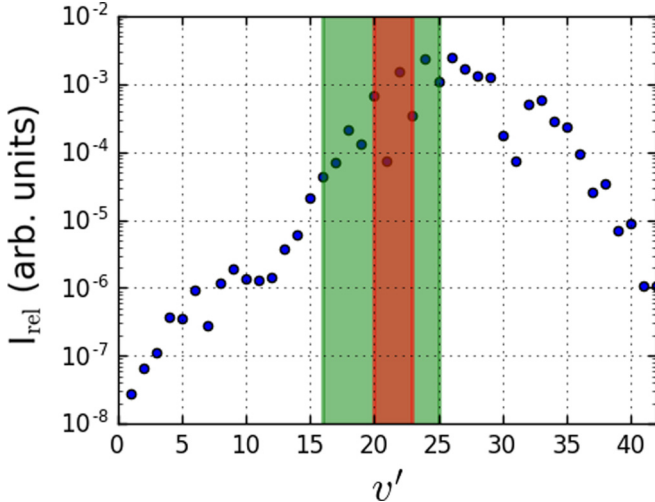

FIG. 6. Calculated STIRAP strengths from $v'' = 43$ to $v'' = 0$ through $C\,{}^1\Sigma^+$, v' as a function of the vibrational level v'. We estimate the STIRAP strength as $I_{rel} = \sqrt{FCF_{down} FCF_{up}}$ [25] in the absence of any information on the transition dipole moments. The wider, green-shaded region represents the states accessible with commercially available green diode lasers, while the enclosed, red-shaded region represents the states accessible with 730-nm diode lasers (the green laser also covers this range). From this $C\,{}^1\Sigma^+$, $v' = 22$ stands out as the best available intermediate state using these lasers, while being the third-best intermediate state overall.

ground-state LiRb molecules. In the present experiment, we exploited the strong mixing in the $A\,{}^1\Sigma^+$–$b\,{}^3\Pi_{0^+}$ complex and we were able to observe $b\,{}^3\Pi_{0^+}$, $v' = 8$–18. Unfortunately, finding more deeply bound vibrational levels will be challenging. We noticed that the amount of mixing between $A\,{}^1\Sigma^+$ and $b\,{}^3\Pi_{0^+}$ states dictates the strength of the state $b\,{}^3\Pi_{0^+}$ depletion resonance, and we expect the mixing to decrease as the states become more deeply bound. Further, the $b\,{}^3\Pi_{0^+}$ $v' = 8 \leftarrow v'' = 2$ transition had a line width of only 1 GHz at full depletion power (compare with the $A\,{}^1\Sigma^+$ $v' = 0 \leftarrow v'' = 2$ transition, which was well over 100 GHz in line width), which makes this a daunting search. However, we expect our molecular constants and those in Refs. [16,18] to be helpful guides.

(3) Our data on mixing between $A\,{}^1\Sigma^+$, $v' = 5$ and $b\,{}^3\Pi_{0^+}$, $v' = 12$ suggests that this state pair is at a nearly 50-50 admixture. This pair of states combines many features that lead us to believe they may be useful in direct short-range PA. The $A\,{}^1\Sigma^+$, $v' = 5$ state has a large FCF overlap with the rovibronic ground state, and the inner turning point of $b\,{}^3\Pi_{0^+}$, $v' = 12$ nearly lines up with the outer turning point of the triplet scattering state. This is a good indicator of states that have potential for use in short-range PA [10]. Finally, the wavelength for PA to this state is 1562 nm, which can be accessed with commercial fiber amplifiers. This is important because we will have watts of PA power available, which will help overcome the weak PA rates common to most short-range PA experiments. In total, $A\,{}^1\Sigma^+$, $v' = 5$ and $b\,{}^3\Pi_{0^+}$, $v' = 12$ may be nearly ideal candidates for producing rovibronic ground-state molecules by short-range PA. As a rough estimate this could produce up to 5×10^4 rovibronic ground-state molecules per second [26].

VII. CONCLUSION

In conclusion, we used molecules produced by PA to a 2(1)-4(1) state to study interesting bound states in LiRb. We used RE2PI to map out the top 20 vibrational levels and 4 lower vibrational levels of the $C\,{}^1\Sigma^+$ state. We used depletion spectroscopy to study the 30 most deeply bound $A\,{}^1\Sigma^+$ vibrational levels and discovered that $A\,{}^1\Sigma^+$–$b\,{}^3\Pi_{0^+}$ mixing is quite strong in this region. We capitalized on the $A\,{}^1\Sigma^+$–$b\,{}^3\Pi_{0^+}$ mixing to study $b\,{}^3\Pi_{0^+}$, $v' = 8$–18. These data will guide our future work in both STIRAP and laser-cooling LiRb molecules.

[1] D. DeMille, Phys. Rev. Lett. **88**, 067901 (2002).

[2] K.-K. Ni, S. Ospelkaus, D. Wang, G. Quéméner, B. Neyenhuis, M. De Miranda, J. Bohn, J. Ye, and D. Jin, Nature **464**, 1324 (2010).

[3] R. Krems, B. Friedrich, and W. C. Stwalley, *Cold Molecules: Theory, Experiment, Applications* (CRC Press, Boca Raton, FL, 2009).

[4] C. Trefzger, C. Menotti, and M. Lewenstein, Phys. Rev. Lett. **103**, 035304 (2009).

[5] B. Capogrosso-Sansone, C. Trefzger, M. Lewenstein, P. Zoller, and G. Pupillo, Phys. Rev. Lett. **104**, 125301 (2010).

[6] S. Dutta, D. S. Elliott, and Y. P. Chen, Europhys. Lett. **104**, 63001 (2014).

[7] A. Altaf, S. Dutta, J. Lorenz, J. Pérez-Ríos, Y. P. Chen, and D. S. Elliott, J. Chem. Phys. **142**, 114310 (2015).

[8] J. Lorenz, A. Altaf, S. Dutta, Y. P. Chen, and D. S. Elliott, Phys. Rev. A **90**, 062513 (2014).

[9] I. Stevenson, D. B. Blasing, Y. P. Chen, and D. S. Elliott, arXiv:1603.02567.

[10] D. B. Blasing, I. Stevenson, Y. P. Chen, and D. S. Elliott, arXiv:1608.06648.

[11] M. Ivanova, A. Stein, A. Pashov, H. Knöckel, and E. Tiemann, J. Chem. Phys. **134**, 024321 (2011).

[12] S. Dutta, A. Altaf, D. S. Elliott, and Y. P. Chen, Chem. Phys. Lett. **511**, 7 (2011).

[13] M. Ivanova, A. Stein, A. Pashov, H. Knöckel, and E. Tiemann, J. Chem. Phys. **138**, 094315 (2013).

[14] I. Stevenson, D. B. Blasing, A. Altaf, Y. P. Chen, and D. S. Elliott, arXiv:1607.04608.

[15] S. Dutta, J. Lorenz, A. Altaf, D. S. Elliott, and Y. P. Chen, Phys. Rev. A **89**, 020702 (2014).

[16] Y. You, C.-L. Yang, Q.-Q. Zhang, M.-S. Wang, X.-G. Ma, and W.-W. Liu, Phys. Chem. Chem. Phys. **18**, 19838 (2016).

[17] J. Kobayashi, K. Aikawa, K. Oasa, and S. Inouye, Phys. Rev. A **89**, 021401(R) (2014).

[18] M. Korek, G. Younes, and S. Al-Shawa, J. Mol. Struct. Theochem. **899**, 25 (2009).

[19] W. Ketterle, K. B. Davis, M. A. Joffe, A. Martin, and D. E. Pritchard, Phys. Rev. Lett. **70**, 2253 (1993).

[20] J. Deiglmayr, A. Grochola, M. Repp, O. Dulieu, R. Wester, and M. Weidemüller, Phys. Rev. A **82**, 032503 (2010).

[21] Converting adiabatic PECs to diabatic PECs means that avoided crossings no longer avoid. Additionally, our conversion is not perfect and resulted in small perturbations to the theoretical vibrational series near $A\,^1\Sigma^+$, $v' = 0$ and $b\,^3\Pi_{0^+}$, $v' = 8$.

[22] R. J. Le Roy, J. Quant. Spectrosc. Radiat. Transfer **186**, 167 (2017).

[23] G. Herzberg and S. Mrozowski, Am. J. Phys. **19**, 390 (1951).

[24] J. Ulmanis, J. Deiglmayr, M. Repp, R. Wester, and M. Weidemüller, Chem. Rev. **112**, 4890 (2012).

[25] For STIRAP, the square root of the Franck-Condon factors matters, because efficient STIRAP relies on high Rabi frequencies. The Rabi frequencies are proportional to the square root of the Franck-Condon factors, unlike transition rates, which are proportional to the raw Franck-Condon factors.

[26] Our estimate is based on calculations of excited-state Franck-Condon overlap with the triplet scattering state done by J. Pérez-Ríos. We used this to determine how strong PA to $A\,^1\Sigma^+$, $v' = 5$ is relative to PA to $d\,^3\Pi_{0^-}$, $v' = 0$, measured in Ref. [10] to be 5×10^3 molecules per second. Finally, we multiplied this PA rate by the branching ratio to $v'' = 0$ and augmented it by the power increase we will get from having much more PA power available. Our estimate is made assuming 1 W of PA power and is by no means an upper limit on the production rate.